



Deposited via The University of Leeds.

White Rose Research Online URL for this paper:

<https://eprints.whiterose.ac.uk/id/eprint/105259/>

Version: Accepted Version

Article:

Cowle, MW, Babatunde, AO and Bockelmann-Evans, BN (2017) The frictional resistance induced by bacterial based biofouling in drainage pipelines. *Journal of Hydraulic Research*, 55 (2). pp. 269-283. ISSN: 0022-1686

<https://doi.org/10.1080/00221686.2016.1212411>

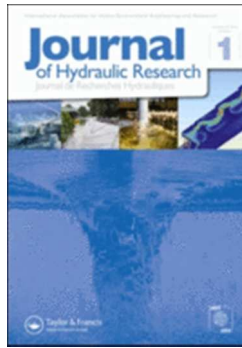
This is an Accepted Manuscript of an article published by Taylor & Francis in *Journal of Hydraulic Research* on 7 September 2016, available online:
<http://dx.doi.org/10.1080/00221686.2016.1212411>

Reuse

Items deposited in White Rose Research Online are protected by copyright, with all rights reserved unless indicated otherwise. They may be downloaded and/or printed for private study, or other acts as permitted by national copyright laws. The publisher or other rights holders may allow further reproduction and re-use of the full text version. This is indicated by the licence information on the White Rose Research Online record for the item.

Takedown

If you consider content in White Rose Research Online to be in breach of UK law, please notify us by emailing eprints@whiterose.ac.uk including the URL of the record and the reason for the withdrawal request.



The frictional resistance induced by bacterial based biofouling within drainage pipelines

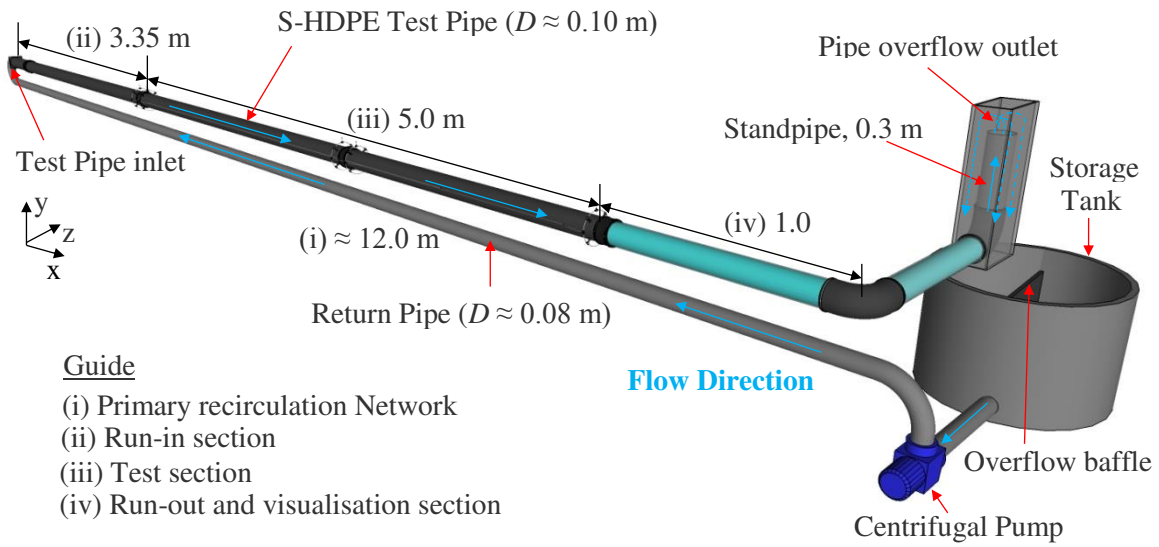
| | |
|-------------------------------|---|
| Journal: | <i>Journal of Hydraulic Research</i> |
| Manuscript ID | TJHR-2015-0061.R3 |
| Manuscript Type: | Research paper |
| Date Submitted by the Author: | 27-Apr-2016 |
| Complete List of Authors: | Cowle, M; Mott MacDonald; Hydro-environmental Research Centre, Cardiff University, Cardiff School of Engineering Babatunde, A; Hydro-environmental Research Centre, Cardiff University, Cardiff School of Engineering Bockelmann-Evans, B; Hydro-environmental Research Centre, Cardiff University, Cardiff School of Engineering |
| Keywords: | biofilm, bacterial based biofouling, drainage pipelines, equivalent roughness, non-universal von Kármán constant, pipe flow |
| JHR Keywords: | Biofilms < Eco-hydraulics, Boundary layer turbulence < Turbulent flows, Sewer hydraulics < Applied fluid mechanics and hydraulic engineering, Pressure and temperature measurements < Instrumentation, measurements and experimental methods, Laboratory studies < Instrumentation, measurements and experimental methods |

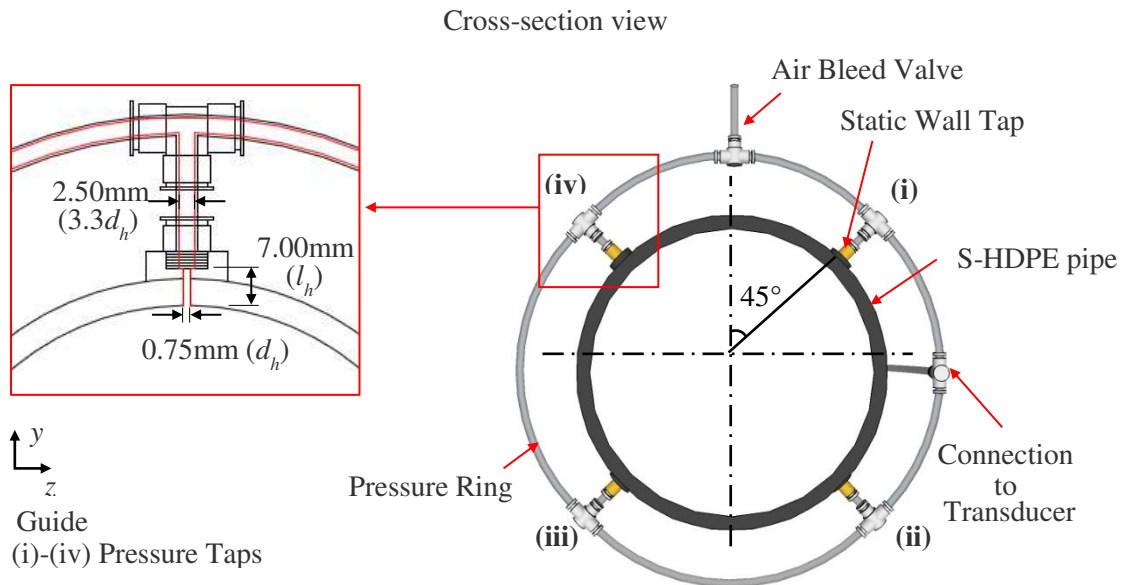
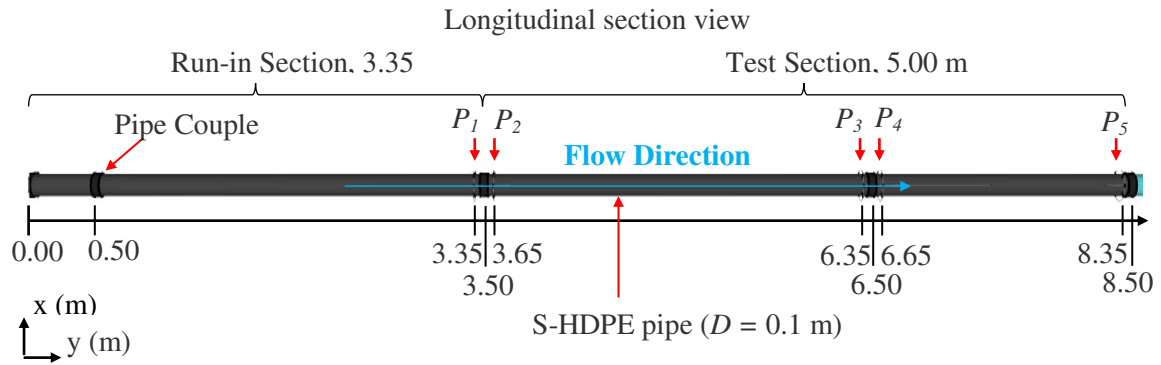
SCHOLARONE™
Manuscripts

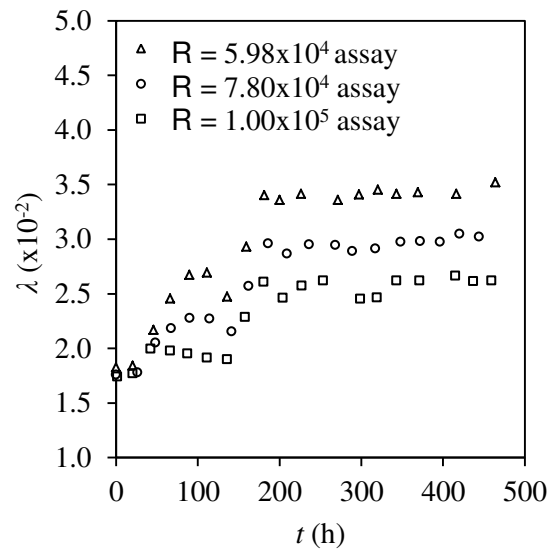
| Assay | R ($\times 10^4$) | \bar{U} (ms^{-1}) | Temperature ($^{\circ}\text{C}$) | v ($\times 10^7$) (m^2s^{-1}) | ρ (kgm^{-2}) | COD (mg l^{-1}) | TOC (mg l^{-1}) | DOC (mg l^{-1}) | TN (mg l^{-1}) | TP (mg l^{-1}) | Ammonium (mg l^{-1}) | Nitrate (mg l^{-1}) | Iron (mg l^{-1}) | Manganese (mg l^{-1}) | |
|------------------------|------------------------|-----------------------------------|---------------------------------------|---|---------------------------------|-------------------------------|-------------------------------|-------------------------------|------------------------------|------------------------------|------------------------------------|-----------------------------------|--------------------------------|-------------------------------------|------|
| R = 5.98×10^4 | Av. | 5.98 | 0.58 | 21.3 | 9.70 | 998.0 | 536.4 | 238.2 | 211.5 | 49.5 | 12.1 | 0.41 | 0.50 | 0.11 | 0.13 |
| | σ | 0.12 | 0.01 | 0.6 | 0.00 | 0.2 | 40.5 | 16.1 | 14.3 | 0.6 | 1.20 | 0.23 | 0.28 | 0.05 | 0.06 |
| | n | 60 | 60 | 60 | 60 | 60 | 20 | 10 | 10 | 2 | 2 | 6 | 6 | 6 | 6 |
| R = 7.82×10^4 | Av. | 7.81 | 0.76 | 21.2 | 9.72 | 998.0 | 545.6 | 251.2 | - | 50.3 | 10.8 | 0.25 | 0.33 | 0.10 | 0.30 |
| | σ | 0.17 | 0.01 | 0.7 | 0.00 | 0.2 | 21.2 | 9.5 | - | 0.4 | 0.8 | 0.23 | 0.28 | 0.07 | 0.20 |
| | n | 60 | 60 | 60 | 60 | 60 | 20 | 20 | - | 2 | 4 | 4 | 4 | 4 | 4 |
| R = 1.00×10^5 | Av. | 1.01 | 0.96 | 21.8 | 9.59 | 997.9 | 548.1 | 241.6 | 190.6 | 51.2 | 11.0 | 0.75 | 1.09 | 0.15 | 0.39 |
| | σ | 0.29 | 0.02 | 0.6 | 0.00 | 0.2 | 23.4 | 12.2 | 9.6 | 0.9 | 0.8 | 0.02 | 0.11 | 0.09 | 0.10 |
| | n | 60 | 60 | 60 | 60 | 60 | 20 | 9 | 9 | 11 | 3 | 4 | 4 | 5 | 5 |

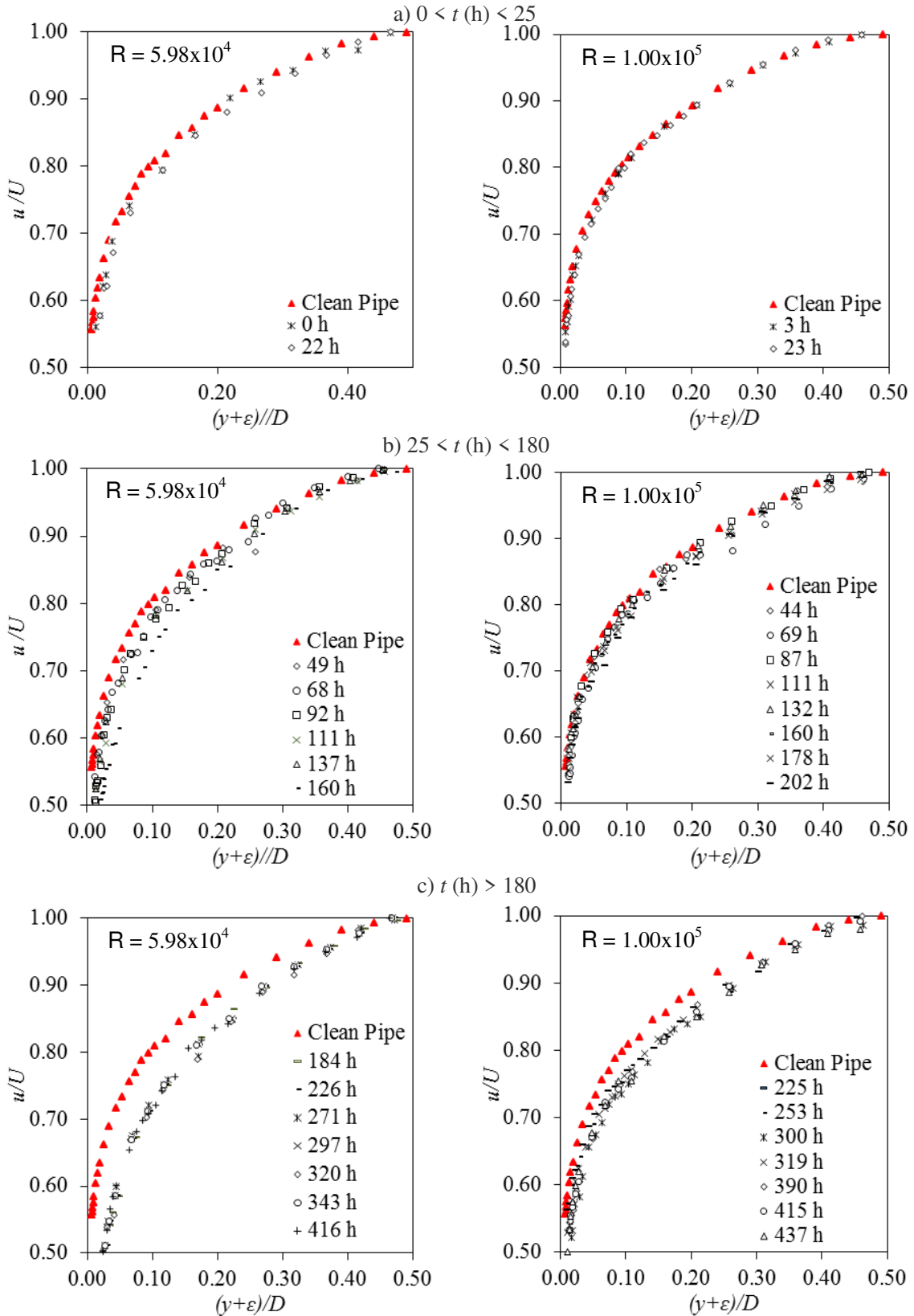
| Parameter | Symbol | Uncertainty (%) | |
|--|-----------|-----------------|-------|
| | | Av. | Max. |
| Fluid density | ρ | 0.02 | 0.03 |
| Fluid kinematic viscosity | ν | 2.39 | 4.14 |
| Reynolds Number (Flowmeter) | R | 10.01 | 15.99 |
| Reynolds Number (Pitot Probe) | | 6.43 | 11.61 |
| Local velocity, near wall region ($y^+ < 50$) | | 3.85 | 4.40 |
| Local velocity, Log-Law region ($50 < y^+ < 300$) | u | 1.21 | 1.79 |
| Local velocity, wake region ($300 < y^+ < R^+$) | | 0.70 | 1.08 |
| Friction factor | λ | 5.15 | 7.30 |
| Shear velocity | u_* | 6.49 | 14.27 |
| Wall shear stress | τ_w | 13.44 | 28.53 |
| Skin friction coefficient | c_f | 4.53 | 15.36 |

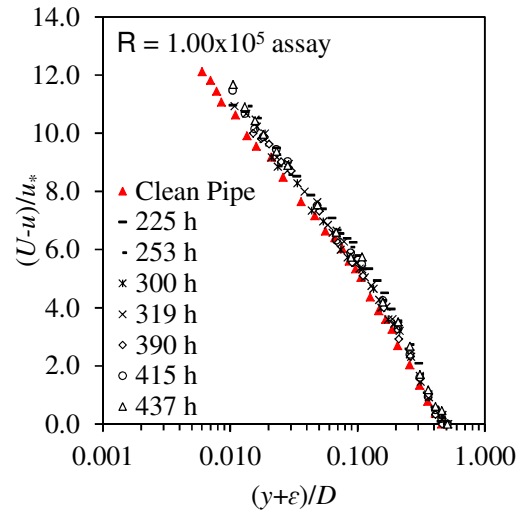
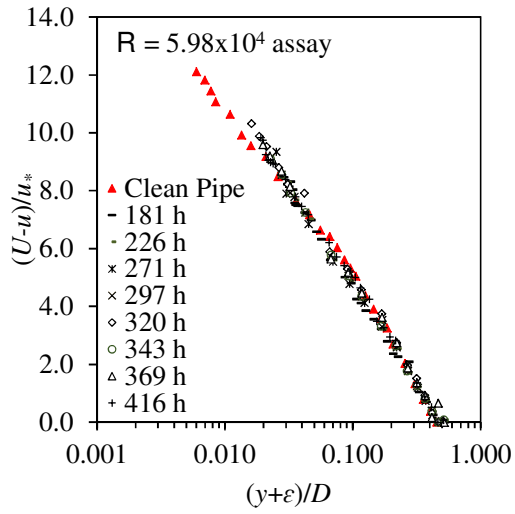
| Assay | λ | u_* (ms^{-1}) | τ_w (Nm^{-2}) | c_f ($\times 10^{-3}$) | k_s (mm) | k_s^+ | |
|------------------------|-----------|-------------------------------|----------------------------------|-------------------------------|---------------|---------|-------|
| $R = 5.98 \times 10^4$ | Av. | 0.034 | 0.038 | 1.42 | 8.54 | 0.637 | 25.05 |
| | σ | 0.000 | 0.001 | 0.07 | 0.12 | 0.023 | 1.76 |
| $R = 7.82 \times 10^4$ | Av. | 0.030 | 0.045 | 2.15 | 7.57 | 0.445 | 20.94 |
| | σ | 0.001 | 0.001 | 0.05 | 0.18 | 0.031 | 1.34 |
| $R = 1.00 \times 10^5$ | Av. | 0.026 | 0.054 | 2.95 | 6.44 | 0.223 | 12.79 |
| | σ | 0.001 | 0.001 | 0.07 | 0.19 | 0.027 | 1.41 |





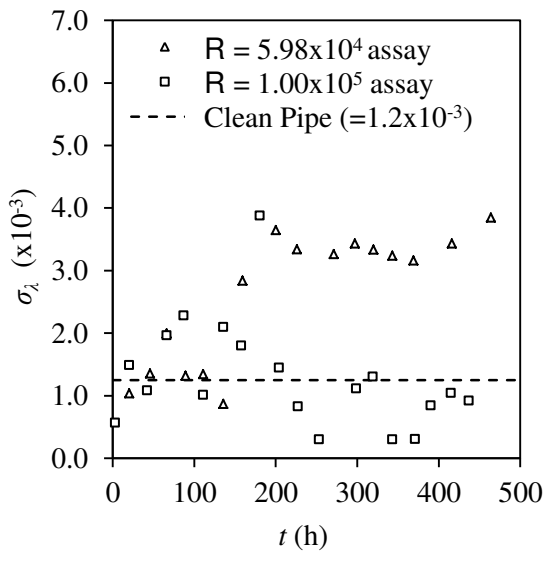


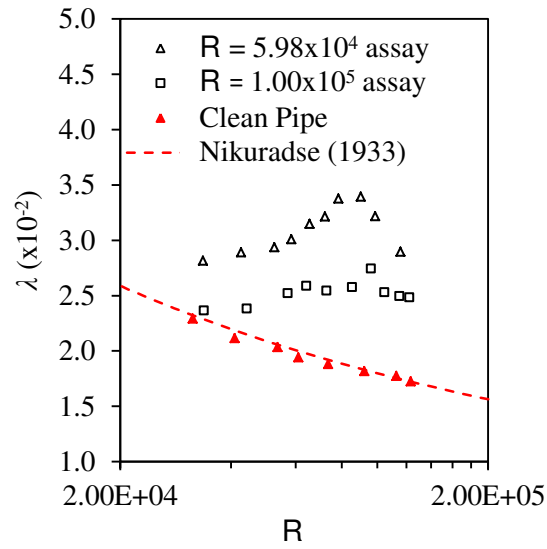


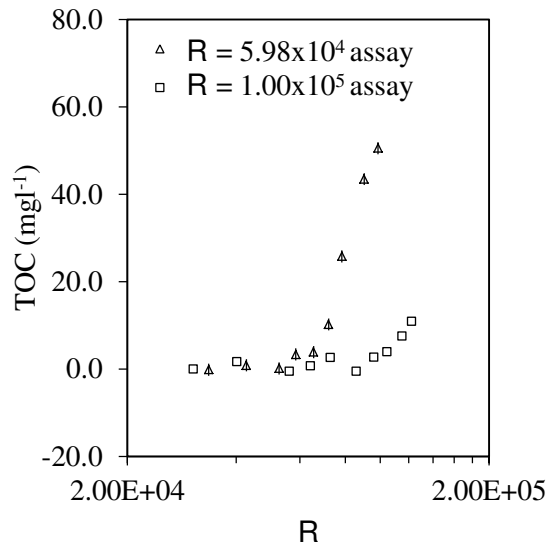


1
2
3
4
5
6
7
8
9
10
11
12
13
14
15
16
17
18
19
20
21
22
23
24
25
26
27
28
29
30
31
32
33
34
35
36
37
38
39
40
41
42
43
44
45
46
47
48
49
50
51
52
53
54
55
56
57
58
59
60

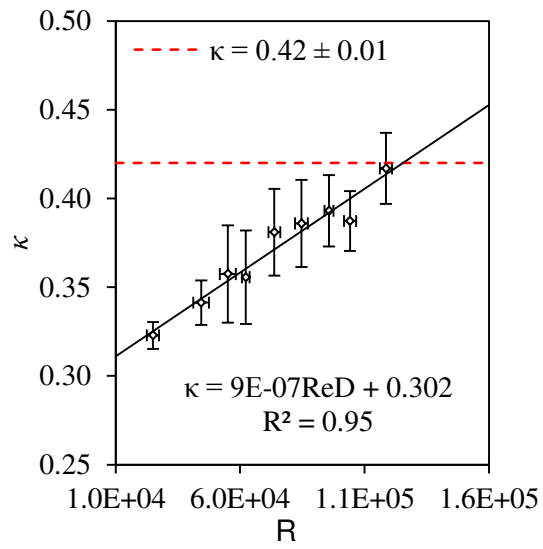
1
2
3
4
5
6
7
8
9
10
11
12
13
14
15
16
17
18
19
20
21
22
23
24
25
26
27
28
29
30
31
32
33
34
35
36
37
38
39
40
41
42
43
44
45
46
47
48
49
50
51
52
53
54
55
56
57
58
59
60



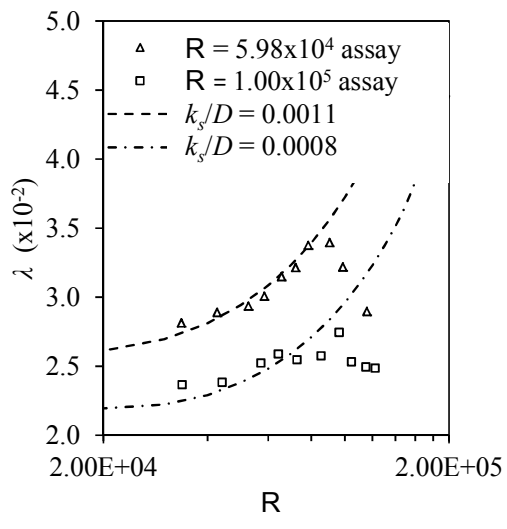


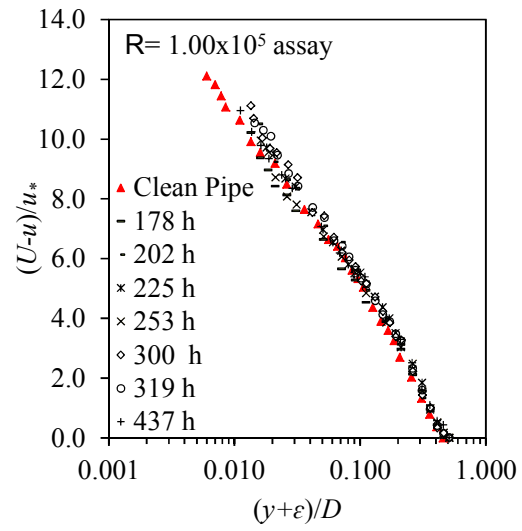
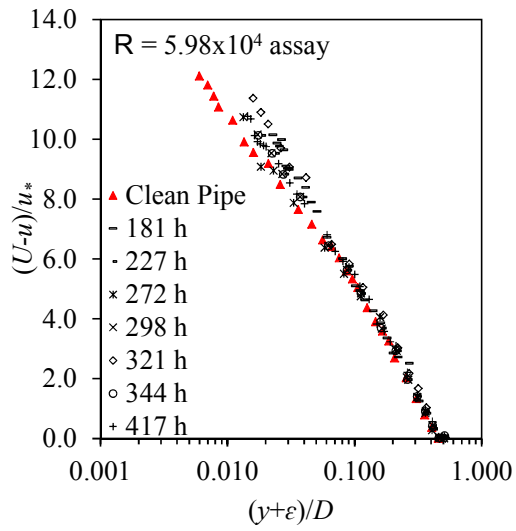


1
2
3
4
5
6
7
8
9
10
11
12
13
14
15
16
17
18
19
20
21
22
23
24
25
26
27
28
29
30
31
32
33
34
35
36
37
38
39
40
41
42
43
44
45
46
47
48
49
50
51
52
53
54
55
56
57
58
59
60



1
2
3
4
5
6
7
8
9
10
11
12
13
14
15
16
17
18
19
20
21
22
23
24
25
26
27
28
29
30
31
32
33
34
35
36
37
38
39
40
41
42
43
44
45
46
47
48
49
50
51
52
53
54
55
56
57
58
59
60





1
2
3 The frictional resistance induced by bacterial based biofouling in
4 drainage pipelines
5
6

7
8 MATTHEW W. COWLE (IAHR Member), Graduate Civil Engineer, *Mott MacDonald,*
9 *Fitzalan House, Cardiff, CF24 0EL, UK* (previously PhD student, *Hydro-environmental*
10 *Research Centre, Cardiff School of Engineering, Cardiff University, The Parade, Cardiff,*
11 *CF24 3AA, UK*)
12

13
14 *Email: matthew.cowle@mottmac.com (author for correspondence)*
15

16
17 AKINTUNDE .O. BABATUNDE, Lecturer, *Hydro-environmental Research Centre, Cardiff*
18 *School of Engineering, Cardiff University, The Parade, Cardiff, CF24 3AA, UK*
19

20
21 *Email: BabatundeA@cf.ac.uk*
22

23
24 BETTINA N. BOCKELMANN-EVANS (IAHR Member), Senior Lecturer, *Hydro-*
25 *environmental Research Centre, Cardiff School of Engineering, Cardiff University, The*
26 *Parade, Cardiff, CF24 3AA, UK*
27

28
29 *Email: Bockelmann-Evans@cf.ac.uk*
30
31

32 *Running Head: The frictional resistance induced by bacterial biofouling*
33
34
35
36
37
38
39
40
41
42
43
44
45
46
47
48
49
50
51
52
53
54
55
56
57
58
59
60

The frictional resistance induced by bacterial based biofouling in drainage pipelines

ABSTRACT

This paper aims at improving the current understanding of bacterial-based biofouling in drainage pipelines. Using a purpose built pipeline facility consisting of a high density polyethylene pipe, biofilms were incubated with synthetic wastewater for 20 days at three steady-state flow regimes. The results obtained have shown that the presence of a biofilm can cause a significant increase in frictional resistance. The magnitude of a biofilm's frictional resistance is a function of the shear conditions under which the biofilm is incubated. In particular, the lower the conditioning shear, the higher the frictional resistance imparted by the biofilm. This is attributed to the thickness and roughness distribution induced by such conditions, and it serves to highlight the problem of characterising a biofilm's effective roughness using a single roughness scale. The study has also supported the earlier finding that the von Kármán constant is non-universal, and is dependent on Reynolds number for biofouled pipes.

Keywords: Biofilm; bacterial based biofouling; drainage pipelines; equivalent roughness; flows in pipes; von Kármán constant

1 Introduction

It is widely acknowledged that population growth, urbanisation and climate change will put significant pressure on pipeline infrastructure over the next century. In particular, the magnitude and intensity of precipitation in extreme events is predicted to increase as a direct result of climate change. The increased runoff and storm water discharge expected has the potential to increase the frequency and magnitude of surcharge and flooding, particularly in highly populated urban areas. Global population growth is likely to further exacerbate the impacts of climate change on sewer systems, especially in urbanised areas where it is predicted that the majority of the growth will be absorbed. The effective management of Drainage Networks (DNs) is therefore of paramount importance to the water industry; and it represents one of the industry's greatest challenges from both an operational and public health standpoint. This challenge is exacerbated by the environmental complexities of DN, which are characterised by highly diverse and variable flow rates, temperatures and their contents. Fouling mechanisms such as bacterial based biofouling, contribute to, and are governed by these inherent complexities. Bacterial based biofouling refers to the natural, albeit sometimes undesirable process through which a complex microbiological slime layer – known as a biofilm – forms upon a surface. Biofilms in pipelines are generally classified on the macro-scale as either low-form gelatinous or filamentous. Their presence can cause a significant

increase in boundary shear stresses and surface roughness (Barton, 2006; Barton Sargison, Buia, Walker, 2008).

The magnitude of the change in surface roughness caused by biofouling is a function of the physical nature of a biofilm (Barton, 2006). Biofilms are viscoelastic in nature and through a vibrating and oscillating action, they have the ability to remove significant amount of energy from a flow field (Andrewartha, 2010; Walker, Sargison, & Henderson, 2013). As a result, a biofilm's effective roughness can be significantly higher than that predicted based upon traditional wall similarity hypothesis, i.e. using the classical Nikuradse-type equivalent sandgrain roughness, k_s , as defined in the Colebrook-White (C-W) equation:

$$\frac{1}{\sqrt{\lambda}} = -2.00 \log \left(\frac{k_s}{3.7D} + \frac{2.51}{R\sqrt{\lambda}} \right) \quad (1)$$

where D is the internal pipe diameter, R is Reynolds number ($=\bar{U}D/\nu$; where \bar{U} is the area-averaged axial flow velocity, and ν is kinematic viscosity ($=\mu/\rho$; where μ is dynamic viscosity and ρ is the specific density)), and λ is the Darcy-Weisbach friction factor:

$$\lambda = \frac{2gDS_f}{\bar{U}^2} \quad (2)$$

where g is the acceleration due to gravity (i.e. 9.81 ms^{-2}), and S_f is the friction slope or pressure gradient ($=dH_f/dx$; where H_f is hydraulic headloss ($=\Delta P/\rho g$, where ΔP is pressure drop) and x is the characteristic length scale (in the streamwise direction). Solving Eq. (1) for k_s yields:

$$k_s = 3.7D \left(10^{\frac{-1}{2\sqrt{\lambda}}} - \frac{2.51}{R\sqrt{\lambda}} \right) \quad (3)$$

The mechanisms by which a biofilm interacts with a fluid along with its physical morphology are governed by the conditions under which it is grown (Stoodley, Dodds, Boyle, & Lappin-Scott, 1998a; Stoodley, Lewandowski, Boyle, & Lappin-Scott, 1998b). There is compelling evidence to suggest that flow hydrodynamics and nutrient availability are the two most influential factors governing biofilm development in pipelines (Stoodley et al., 1998a, Lauchlan, Forty, & May, 2005). However, in DN's where it is likely that sufficient nutrients would be available; flow hydrodynamics will be the primary controlling factor due to its potential to remove existing biofilms, and/or counteract further growth. Nonetheless, there is an inherent link between flow hydrodynamics and nutrient availability on biofilm development; and this is due to their combined influence on mass transfer and diffusion. The mass transfer and diffusion potential of a system is predominantly controlled by the level of turbulence in the flow (i.e. R).

The prevailing conditions in a typical DN imply that the presence of a biofilm is realistically unavoidable. Consequently, the accurate assessment of a biofouled surface is

imperative for efficient pipeline design and effective control strategies. However, this is not possible through the application of conventional design approaches which utilise traditional frictional relationships and roughness scales. In particular, in their current forms Eq. (1) and k_s have been deemed inadequate for biofouled surfaces (Barton, 2006; Lambert, Edwards, Howie, Gilio, & Quinn, 2009; Perkins, Henderson, Walker, Sargison, & Li, 2014). It has been widely suggested that the complex surface dynamics of a biofilm cannot be adequately defined by a single one-dimensional parameter, such as k_s (Andrewartha, 2010; Barton, 2006). However, as such a parameter (or series of parameters) has yet to be successfully formulated, the Nikuradse equivalent sandgrain height was used within this study to define k_s .

Lambert et al. (2009) used experimental observations on freshwater biofilms to obtain a modified C-W equation (Eq. (4)), which is aimed at addressing the inadequacy of Eq. (1), i.e.:

$$\frac{1}{\sqrt{\lambda}} = -\frac{1}{\sqrt{8.08\kappa}} \ln \left(\frac{k_s}{0.85D} + \frac{2.51}{R\sqrt{\lambda}} \right) \quad (4)$$

Lambert et al. (2009) found that for biofouled pipes, the von Kármán constant κ , which is a fundamental part of the Eq. (1), was non-universal, dependant on R , and lower than the conventional value (i.e. $\kappa = 0.42$). Solving Eq. (4) for k_s yields:

$$k_s = 0.85D \left(e^{\frac{-1\sqrt{8.08\kappa}}{\sqrt{\lambda}}} - \frac{2.51}{R\sqrt{\lambda}} \right) \quad (5)$$

Similar observations were reported by Perkins et al. (2014) for biofilms incubated in a hydropower system. However, these studies assessed a very specific set of environmental conditions; and in the case of Lambert et al. (2009), a very limited range of flow regimes (at low R values). Furthermore, the environmental conditions in a hydropower or freshwater system are inherently different to those found in DNs; and this would be reflected in the respective system's biofilm. This ultimately affects the broader application of the reported observations, particularly with respect to DNs. Nonetheless, the existence of a non-universal log-law is not a new concept, as there is debate within the classical theory as to whether κ is truly independent of R (Wei, Schmidt, & McMurtry, 2005). The highly dynamic nature of a biofouled surface will undoubtedly add an additional layer of complexity to the debate. The implication of a non-universal κ on roughness and flow rate determination (using Eq. (1)) could be considerable. This would be reflected in pipeline design through pipe sizing; and this could have financial and environmental implications especially if the pipe is oversized as a result (Cowle, Babatunde, Rauen, & Bockelmann-Evans, 2014). The impact of a non-universal κ would also be detrimental to wall similarity techniques, particularly with respect to their ability to effectively establish the local roughness for biofouled surfaces. This is

1
2
3 because these techniques which are commonly used to determine parameters such as wall
4 shear velocity u_* by fitting experimental data to the law of the wall (Eq. (6)), are reliant on
5 the existence of a universal log-law:
6

$$\frac{u}{u_*} = \frac{1}{\kappa} \ln(Y^+) + B$$

7
8
9
10
11 or
$$\frac{u}{u_*} = \frac{1}{\kappa} \ln(Y^+) + 5.6 - \Delta U^+ \quad (6)$$

12
13 where u is the local mean velocity, Y^+ is the normalised wall distance ($=u_*y/\nu$, where y is the
14 wall distance), B is Nikuradse's roughness function which assumes different values
15 depending on the flow regime (for fully rough flow $B = 8.48$), and ΔU^+ is the roughness
16 function which represents the shift in the velocity profile from the smooth wall profile, and
17 increases with increasing surface roughness. As a result, the frictional data derived from wall
18 similarity techniques are highly sensitive to κ (Wei et al., 2005). The current prevailing
19 understanding of biofilm-flow interactions is predominantly based upon observations
20 established from wall similarity techniques, and thus a universal log-law (Andrewartha, 2010;
21 Barton, 2006; Walker et al., 2013). The potential non-universality of κ could bring the
22 conclusions of these studies into question.
23

24
25
26
27
28
29
30
31
32
33
34
35
36
37
38
39
40
41
42
43
44
45
46
47
48
49
50
51
52
53
54
55
56
57
58
59
60
Ultimately, the inadequacies in current design practices and hydraulic theory are a
reflection of the current state of scientific understanding of biofouling in DN's (Cowle et al.,
2014). The increasing awareness and emphasis on sustainability within the water industry,
with respect to both the capacity and efficiency of existing networks and future installations,
means that it is now more important than ever to change the perception of biofouling and
address the inadequacies in current pipe design approaches.

The aim of this study was to evaluate the impact of biofouling on the surface
roughness of a drainage pipe within a controlled laboratory environment. This would provide
a platform through which the inadequacies in current pipe design approaches could be
addressed. To this effect, the specific objectives of the study were to comprehensively
determine the impact of biofouling on surface roughness and mean-velocity; investigate the
impact of flow shear on biofilm development; and examine whether κ is non-universal for
biofouled pipes.

2 Material and methods

2.1 Experimental facility

The experiments reported herein were conducted in a purpose built pilot scale pipeline
facility, located in the Hydraulics Laboratory, at Cardiff University School of Engineering.
The facility was designed and developed as an open loop, recirculating system for the specific

1
2
3 purpose of studying biofilm-flow interaction in DNs, over a wide range of flow conditions. It
4 was fabricated mainly from high density polyethylene (HDPE), and it consisted of a storage
5 tank (350 l), working and recirculation parts. The fluid in the pipeline was recirculated by a
6 2.25 kW single phase centrifugal water pump (*Clarke CPE30A1*). The pump is capable of
7 operating over the range of $0.3 \text{ ms}^{-1} < \bar{U} < 1.3 \text{ ms}^{-1}$ (or $3.0 \times 10^4 < R < 1.30 \times 10^5$, based on a
8 fluid temperature of 20°C). The fluid temperature in the system was maintained by an external
9 cooling unit (*D&D, DC-750*), and it was measured by two universal temperature probes
10 (model: *LabJack EI-1034*). The probes had a typical accuracy of $\pm 0.22^\circ\text{C}$ at room
11 temperature, and they were calibrated under non-flow and flow conditions using a mercury
12 thermometer which had an accuracy of $\pm 0.10^\circ\text{C}$. Temperature control is essential in both
13 biofilm and boundary layer investigations, for the purpose of environmental and R control.
14 The fluid temperature in the facility was maintained at $21.5 \pm 0.9^\circ\text{C}$ and this is representative
15 of the temperature found in typical European DNs during the summer (i.e. $18\text{-}22^\circ\text{C}$) (Cipolla
16 & Maglionico, 2014).
17
18
19
20
21
22
23
24

25
26 *[Insert Fig. 1]*
27
28

29 The working part of the facility was 9.5 m in length and it consisted of a test pipe (8.5
30 m) and a visualisation pipe (1.0 m). The test pipe comprised of four individual solid wall high
31 density polyethylene (S-HDPE) pipe segments. The discrete pipe segments were carefully
32 aligned and connected by flexible pipe coupling in a way that ensures a smooth transition
33 between the segments. Nonetheless, it was inevitable that the joints would cause some
34 disruption to the velocity fields in the system. An S-HDPE pipe was selected due to its
35 extensive use in the water industry, especially within the UK and modern projects. The inner
36 diameter of the test pipe was measured at 8 axial locations and at 6 different positions along
37 the length of the pipeline. The inner diameter was determined to be $102.08 \pm 0.44 \text{ mm}$.
38
39
40
41
42
43
44

45
46 *[Insert Fig. 2]*
47
48

49 As shown in Fig. 2, the test pipe consisted of a run-in section and a test section. The
50 run-in section was 3.35 m (or $34 D$) long and it corresponded to the region of $0.00 \text{ m} < x <$
51 3.35 m . Using the criteria outlined by Zagarola and Smits (1998), the length of the run-in
52 section was deemed sufficient for fully developed mean flow to be obtained in the test
53 section. The test section was 5.0 m in length and was located between $3.35 \text{ m} < x < 8.35 \text{ m}$.
54

55 A hydrodynamic evaluation of the test pipe under non-fouled conditions over the
56 range of $3.15 \times 10^4 < R < 1.23 \times 10^5$ indicated that it had a k_s value of 0.01 mm. A surface is
57 considered hydraulically smooth if the roughness Reynolds number, $k_s^+ (=k_s v/u_*)$ is less than
58
59
60

1
2
3 or equal to five (Nikuradse, 1933). The maximum value of k_s^+ , which corresponds to the
4 maximum R investigated (i.e. $R = 1.23 \times 10^5$) was found to be 0.51. Consequently, the test
5 pipe was considered to be hydraulically smooth.
6
7

8 9 2.2 Measurements and instrumentation

10 11 *Volumetric flow rate*

12
13 The volumetric flow rate in the facility was recorded using a “time of flight” ultrasonic
14 flowmeter (Nixon CU100). The meter had a reading accuracy of $\pm 1.5\%$ and it was located in
15 the recirculation part of the system. The flow rate, Q recorded by the ultrasonic flowmeter
16 was verified against the Q values established from local mean-velocity data using a Pitot
17 probe and conservation of mass principles. The diameter of the Pitot probe, d_p ($=1.0$ mm)
18 used to measure the mean-velocity data limited the spatial resolution near the wall to
19 approximately 0.5 mm. Consequently, a near wall correction was required, especially for high
20 R values (Zagarola, 1996). The values of Q determined from the flowmeter and Pitot probe
21 were found to have a strong correlation, with a coefficient of determination R^2 of 0.92.
22
23
24
25
26
27

28 29 *Pressure gradient*

30
31 As the flow in the test section was fully developed, the frictional resistance of the pipe can be
32 accurately determined from the system’s pressure gradient (PG) by applying simple
33 equilibrium considerations. The test section’s PG was measured using a series of static wall
34 tappings located at various circumferential and longitudinal positions as shown in Fig. 2. In
35 order to minimise the impact of the wall tappings on the external flow field, the tappings were
36 designed in accordance with the recommendations outlined by McKeon and Smits (2002).
37 The key size characteristics of the wall tappings were $d_h = 0.75$ mm, $d_h/D = 7.35 \times 10^{-3}$, $l_h = 7.0$
38 mm, $l_h/d_h = 9.3$, $d_c = 2.5$ mm and $d_c/d_h = 3.33$; where d_h is the wall tappings’ diameter, l_h is the
39 wall tappings’ length and d_c is the diameter of the connection to pressure gauge.
40
41
42
43
44

45 Four wall tappings linked in a pressure ring arrangement were located at five
46 streamwise locations (i.e. P_1, P_2, P_3, P_4, P_5 , as shown in Fig. 2) along the test section. The
47 pressure ring arrangement allowed a circumferential average pressure to be determined at
48 each location; this reduced potential errors caused by uneven and unstable flow distributions
49 (Barton, 2006). During a typical PG traverse, the time-averaged static pressure at each of the
50 five streamwise locations was recorded at least 4 times and an average value determined. The
51 wall tapping correction criteria outlined by McKeon and Smits (2002) was applied to all static
52 pressure measurements recorded within the study.
53
54
55
56
57
58
59
60

Local velocity measurements

A Pitot probe located at P_5 (i.e. $x = 8.35$ m) was used to obtain all time-averaged velocity profile traverses within the test pipe. The probe's aperture was square ended and 1.0 mm in diameter; and it was located in the same plane as the wall tapings at P_5 . However, the main body of the probe was offset from the plane by 30.0 mm in a downstream direction; and this minimised any potential flow disruptions caused by the probe. A watertight gland allowed the probe to freely traverse 93% of the pipe's vertical plane. A wall origin, $y = 0$, was chosen at the invert side of the pipe. The distance along the pipe's vertical centreline relative to the wall origin was accurately determined using a digital height gauge (*Rapid AK9636D*), which had an accuracy of ± 0.01 mm. A typical velocity traverse consisted of at least 45 logarithmically spaced wall-normal positions. Several corrections were applied to all pressure measurements recorded by the Pitot probe and static wall tapping to account for the effects of viscosity, velocity gradient, the presence of the wall, and turbulence (McKeon, Li, Jiang, Morrison, & Smits, 2003).

The wall similarity technique outlined by Perry and Li (1990) – referred to herein as the PL method – was used to determine the local frictional conditions at P_5 . The PL method has been used to evaluate biofouled surfaces (Andrewartha, 2010; Walker et al., 2013), and it is known to consistently produce highly accurate values of local u_* (Walker, 2014). The von Kármán constant applied during this analysis was 0.42. The Nikuradse's roughness function was determined using the procedure outlined by Ligami and Moffat (1986). To establish u_* using the PL method, the exact location of the wall must be known. However, this was difficult to achieve given the position of the probe within the test pipe. Consequently, a wall origin correction, ε , was applied. An adaptation of the method proposed by Perry and Joubert (1963) was integrated into the PL method in order to solve for ε and u_* simultaneously using an iterative approach.

Pressure transducers and data acquisition

All pressure measurements were obtained using three high accuracy pressure transducers (*Omega PXM409-070HG10V*), designated 1 to 3; all of which had a full scale accuracy (including effects of linearity, hysteresis and repeatability) of $\pm 0.08\%$ (or ± 0.57 mmH₂O (at 20°C)). The pressure transducers were regularly calibrated to within ± 0.5 mm using individual wall mounted water manometers. Transducers 1 and 2 were used to record the pressure measurements required for each of the PG and velocity profile traverses. Transducer 3 always recorded the static pressure at location P_1 during each of the respective traverses; for the purpose of removing any temporal variations observed during testing.

1
2
3 For each measurement interval within each of the PG and velocity profile traverses;
4 the pressure, temperature and flow rate were simultaneously recorded by their respective
5 devices and streamed to a desktop PC at a frequency of 100 Hz using a multifunction 24-bit
6 datalogger (*LabJack U6-Pro*). Appropriate sampling times were derived for each of the
7 variables using a cumulative time-averaged approach. For each discrete measurement, a
8 setting time of 30 s and an acquisition time of 24 s was used to ensure transients had settled,
9 and accurate time averaged pressure measurements could be attained.
10
11
12
13

14 2.3 Operating conditions

15
16
17 Biofilms were incubated in the facility with a synthetic wastewater under full bore and steady
18 state conditions within three separate flow regime assays, namely: the $R = 5.98 \times 10^4$ (or $\bar{U} =$
19 0.60 ms^{-1}) assay; $R = 7.82 \times 10^4$ (or $\bar{U} = 0.75 \text{ ms}^{-1}$) assay; and $R = 1.00 \times 10^4$ (or $\bar{U} = 1.00 \text{ ms}^{-1}$)
20 assay. The flow conditions within the respective assays are common in DNs in the UK,
21 particularly in pumping/force mains which typically operate full bore and between the range
22 of $0.6 \text{ ms}^{-1} < \bar{U} < 1.0 \text{ ms}^{-1}$ (Lauchlan et al., 2005). The maximum recorded variation in R was
23 $\pm 3\%$, this indicates that the flow conditions within the respective assays were reasonably
24 homogenous. The shear stress, τ_w acting on the biofilm was $\tau_w = 1.42 \text{ Nm}^{-2}$ for the $R =$
25 5.98×10^4 assay, $\tau_w = 2.15 \text{ Nm}^{-2}$ for the $R = 7.82 \times 10^4$ assay, and $\tau_w = 2.95 \text{ Nm}^{-2}$ for the $R =$
26 1.00×10^4 assay. These values are based upon the initial conditions (i.e. without fouling) and
27 the principle that the primary force acting on the biofilm was the shear force generated by the
28 flow (Stoodley, Cargo, Rupp, Wilson, & Klapper, 2002). The internal hydraulic retention
29 time in the facility during the three flow assays was at least 73 s and therefore the systems
30 were considered to be well-mixed.
31
32
33
34
35
36
37
38

39 The synthetic wastewater was prepared according to the specification outlined by the
40 Organisation for Economic Cooperation and Development (OCED, 1984), which provided
41 nutrient conditions that are representative of those found in typical DNs in Europe. The
42 wastewater had the following composition: 320 mg l^{-1} of Peptone; 220 mg l^{-1} of meat extract
43 (540 mg l^{-1} as Chemical Oxygen Demand (COD)); 30 mg l^{-1} of Urea ($\text{CH}_4\text{N}_2\text{O}$) (50 mg l^{-1} as
44 Total Nitrogen, (TN)); 12 mg l^{-1} of di-potassium hydrogen phosphate (KH_2PO_4) (10 mg l^{-1} as
45 Total Phosphorus (TP)); 7 mg l^{-1} of sodium chloride, 4 mg l^{-1} of Calcium Chloride Dihydrate
46 ($\text{CaCl}_2 \cdot 2\text{H}_2\text{O}$); and 2 mg l^{-1} of Magnesium Sulfate Heptahydrate ($\text{MgSO}_4 \cdot 7\text{H}_2\text{O}$). The pH,
47 Total Organic Carbon (TOC) and Dissolved Organic Carbon (DOC) of the prepared wastewater
48 was 7.95 ± 0.15 , 244 mg l^{-1} and 201 mg l^{-1} , respectively. The physico-chemical properties of
49 the wastewater within the three flow assays are presented in Table 1.
50
51
52
53
54

55 The three flow assays ran for 20 d (480 h). Based on the nutrient conditions, this was
56 deemed sufficient for the biofilms to reach a state of equilibrium, at least in terms of their
57
58
59
60

1
2
3 frictional resistance (Andrewartha, 2010; Lambert et al., 2009). Prior to the experimental
4 work, the entire facility was disinfected using a concentrated chlorine solution, and sodium
5 thiosulfate was used to neutralise any residual chlorine in the facility post disinfection.
6
7

8
9 *[Insert Table 1]*
10

11 2.4 *Experimental uncertainty*

12 The uncertainties associated with the friction parameters measured and calculated within the
13 current study are given in Table 2. The uncertainties were determined from repeatability test
14 and they represent a 95% confidence interval. The repeatability tests were undertaken under
15 non-fouled conditions over the range of $3.15 \times 10^4 < R < 1.23 \times 10^5$ (at increments of $R \approx$
16 1.00×10^4). Each R increment included a PG and velocity profile traverse and was repeated at
17 least three times.
18
19
20
21
22
23

24 *[Insert Table 2]*
25
26

27 The uncertainties listed in Table 2 for the non-fouled pipe represent the worst case
28 conditions for the facility; and this was due to the smoothness of the non-fouled pipe and the
29 R values assessed. Higher Reynolds numbers, i.e. in excess of $R = 1.30 \times 10^5$ which would
30 have improved the experimental uncertainties listed in Table 2 could not be achieved using
31 the facility in its current arrangement. Similarly, a test section with a greater overall length
32 which could also have improved the experimental uncertainties, could not be achieved due to
33 laboratory restrictions.
34
35
36
37
38

39 **3 Results and discussion**

40 3.1 *General description of fouled pipes*

41 The biofilms incubated with synthetic wastewater within the current study displayed a
42 predominantly low-form gelatinous structure. Filamentous type development was observed
43 but very rarely, with filaments seldom exceeding 10 mm. The fouled pipes showed various
44 amounts of microbial material with very different morphologies depending on the
45 conditioning. Typically, the biofilm incubated at high shear (i.e. in the $R = 1.00 \times 10^5$ assay)
46 had a seemingly more uniform coverage than the biofilm incubated at low shear (i.e. in the R
47 $= 5.98 \times 10^4$ assay), which had a more isolated structure. Molecular analysis of the biofilms
48 showed that they were diverse arrays of microbial cells, embedded within an extracellular
49 polymer matrix of which carbohydrates dominated. Polymerase Chain Reaction-Denaturing
50
51
52
53
54
55
56
57
58
59
60

1
2
3 Gradient Gel Electrophoresis (PCR-DGGE) indicated that the biofilms were dominated by
4 *Bacteria* and in particular, members of the phyla *Alphaproteobacteria*, *Betaproteobacteria*,
5 *Actinobacteria*, *Bacteroidetes* and *Firmicutes*. These species are commonly found in DNAs and
6 as a result, the biofilms were considered representative of those found in real systems, at least
7 in terms of bacterial dominance (Santo Domingo, Revetta, Iker, Gomez-Alvarez, Garcia,
8 Sullivan, & Weast, 2011).
9
10
11

12 3.2 Impact on frictional resistance

13
14 A complete set of PG and mean-velocity traverses were taken at least 3 times a day during
15 each of the biofilm incubation phases, with the exception of the $R = 7.82 \times 10^4$ assay where
16 only PG data was collected. A total of 60 PG and mean-velocity (if applicable) profiles were
17 taken during the incubation phase of three flow assays. The influence of biofilm development
18 on frictional resistance in the form of λ over time t is depicted in Fig. 3. The values of λ
19 presented in Fig.3 for the three flow assays were determined from the system's PG using Eq.
20 (2), where S_f was derived from a linear fit of the profiles of static pressure and therefore, it
21 represents the space-averaged conditions over the entire test section. The static pressure
22 profiles recorded within this study for all the fouled pipes, at all flow rates and time intervals
23 were always a linear function.
24
25
26
27
28
29
30
31

32 [Insert Fig. 3]

33
34
35 The increase in frictional resistance, as indicated by the increase in λ caused by the
36 biofilm development was significant, particularly with respect to the initial non-fouled
37 conditions. This is consistent with the findings outlined previously within the literature
38 (Barton et al., 2008). The observed increases in frictional resistance would have potentially
39 resulted in a reduction in Q of between 15-22% had the pressure drop been held constant in
40 each of the respective flow assays. It is evident from Fig. 3 that λ begins to depart from the
41 non-fouled value after just 25 h of incubation. The biofilms reached a state of equilibrium, in
42 terms of their frictional development after approximately 180 h (see Fig. 3). A summary of
43 the frictional conditions recorded after the biofilms had reached a state of equilibrium is
44 presented in Table 3, where c_f is the skin friction coefficient. The values of k_s presented in
45 Table 3 were determined using the traditional C-W equation (i.e. Eq. (3)) and therefore, they
46 should be viewed with caution as a result of the equation's documented inadequacies in
47 evaluating biofouled surface (as discussed previously in section 1).
48
49
50
51
52
53
54
55

56 [Insert Table 3]

1
2
3
4
5
6
7
8
9
10
11
12
13
14
15
16
17
18
19
20
21
22
23
24
25
26
27
28
29
30
31
32
33
34
35
36
37
38
39
40
41
42
43
44
45
46
47
48
49
50
51
52
53
54
55
56
57
58
59
60

It is evident from Table 3 and Fig. 3 that the highest values of λ were measured in the $R = 5.98 \times 10^4$ assay where λ plateaued at 0.034. The lowest values of λ were measured in the $R = 1.00 \times 10^5$ assay where λ plateaued at 0.026. The $R = 7.82 \times 10^4$ assay represented the intermediate. Single factor analysis of variances (ANOVAs) conducted on the three flow assay datasets indicated that the differences in λ between the respective assays were statistically significant, within the experimental uncertainty. The significance level of all ANOVAs was set at $\alpha = 0.05$.

Dimensionless mean-velocity profiles are presented in Fig. 4 for the range of $0 \leq (y+\varepsilon) \leq r$ (where r is the pipe radius ($=D/2$)). It can be seen that the biofilms caused a gradual shift in the velocity profiles associated with increasing surface roughness. This is in agreement with observations of Walker et al. (2013) for biofilms incubated in a hydropower channel for between 2-52 weeks, at $\bar{U} \approx 1.0 \text{ ms}^{-1}$. Once the biofilms had reached a state of equilibrium, the respective profiles appeared to collapse well onto a single curve (see Fig. 4c). Varying degrees of roughness can be observed in Fig. 4; and typically, the biofilm cultivated in the $R = 5.98 \times 10^4$ assay had the greatest influence on roughness, as exhibited by the greatest shift away from the non-fouled data. The mean-velocity data is presented in velocity defect form in Fig. 5. It is evident from Fig. 5 that the non-fouled and fouled data collapsed well onto a single curve in the outer region of the boundary layer. This suggests that the presence of a biofilm did not affect the mean-flow structure in the outer region and therefore it provides support for Townsend's wall similarity hypothesis. This has also been observed within the literature for freshwater and marine biofilms (Walker et al., 2013).

[Insert Fig. 4]

[Insert Fig. 5]

It is evident that the frictional resistance induced by a biofilm is a function of the biofilm's conditioning. In particular, the lower the conditioning R , the greater the frictional resistance imposed by the biofilm. This is to be expected, as the overall thickness of a biofilm is heavily dependent on the shear conditions in which it is incubated; and typically, the higher the conditioning shear the thinner the biofilm (Barton, 2006; Celmer, Oleszkiewicz, Cicek, 2008). As a biofilm's thickness defines to some extent the physical and effective roughness of a biofouled surface, the thinner the biofilm, the lower the frictional resistance expected (Andrewartha, 2010; Barton, 2006). Naturally, the opposite is true of thicker biofilms.

Furthermore, the mass transfer and drag limitation potentials associated with lower R values would typically foster a more isolated and irregularly distributed biofilm (Stoodley et

1
2
3 al., 1998a). Such a roughness distribution would induce a higher overall frictional resistance
4 than that imposed by a uniformly distributed structure (Andrewartha, 2010; Stoodley et al.,
5 2002). This could further explain the relatively high nature of the frictional data recorded in
6 the $R = 5.98 \times 10^4$ assay. Alternatively, the increased mass transfer and diffusion potentials
7 associated with higher R values would have induced a more uniformly distributed biofilm
8 (Celmer et al., 2008; Stoodley et al., 2002). The increased uniformity coupled with the limits
9 imposed on maximum thickness by the inherently high drag could explain the low values of λ
10 recorded in the $R = 1.00 \times 10^5$ assay.
11

12 The irregularity of the biofilm's space-averaged roughness distribution was evaluated
13 by examining each part of the test section discreetly (i.e. P_1 - P_5 , P_1 - P_4 , P_1 - P_3 etc.). Figure 6
14 illustrates the standard deviation in λ for the $R = 5.98 \times 10^4$ and $R = 1.00 \times 10^5$ assays. The
15 average standard deviation in λ determined under non-fouled conditions of 1.25×10^3 is also
16 presented in Fig. 6 for reference purposes. It is evident from Fig. 6 that the variation in space-
17 averaged conditions along the test section after the biofilms had reached a state of
18 equilibrium, was far greater in the $R = 5.98 \times 10^4$ assay than in the $R = 1.00 \times 10^5$ assay. This
19 was supported by single factor ANOVAs conducted on the respective flow assays (where $\alpha =$
20 0.05) which indicated that the differences in the values of λ recorded along the test section in
21 the $R = 5.98 \times 10^4$ assay were statistically significant, whereas the ANOVAs performed on the
22 $R = 1.00 \times 10^5$ assay data showed that the differences in values of λ were statistically
23 insignificant. The observed variations in the space-averaged values of λ supports the
24 assumption that biofilm's overall coverage in the $R = 5.98 \times 10^4$ assay was more irregular and
25 thus less uniform (over the length of the system), than the respective coverage in the $R =$
26 1.00×10^5 assay. The observed heterogeneity of a biofilm's roughness serves to highlight the
27 problem of characterising a biofilm's effective roughness using a single scale, i.e. k_s .
28
29
30
31
32
33
34
35
36
37
38
39
40
41
42

43 [Insert Fig. 6]
44
45
46

47 3.3 Influence of Reynolds number on mature biofilm development

48 Once the biofilms incubated in the $R = 5.98 \times 10^4$ and $R = 1.00 \times 10^5$ assays had reached a state
49 of equilibrium in terms of their frictional resistance, they were subjected to varying flow
50 regimes (over the range of $3.05 \times 10^4 < R < 1.23 \times 10^5$). A total of 10 R increments were
51 assessed within this phase which will be referred to as the mature testing phase. A complete
52 set of PG and mean-velocity traverses were recorded for each of the fouled pipes at each R
53 increment. A total of 62 PG and mean-velocity profiles were recorded during the mature
54 testing phase. This took place after approximately 480-500 h of incubation, and it lasted for
55
56
57
58
59
60

1
2
3 about 12-15 h. An unforeseen complication which led to the death of the biofilm incubated in
4 the $R = 7.82 \times 10^4$ assay prior to the 500 h mark precluded it from this phase of testing.
5

6 The influence of R on λ is illustrated in Fig. 7. The relationships between R and λ
7 depicted in Fig. 7 for the respective fouled pipes are evidently different to that expected based
8 on standard convention (i.e. Eq. (1)). In particular, it is evident from Fig. 7 that λ increases
9 with increasing R . For the $R = 5.98 \times 10^4$ assay, λ increased to a maximum of 3.34×10^{-3} at $R =$
10 9.02×10^4 ; whereas for the $R = 1.00 \times 10^5$ assay, λ increased to a maximum of 2.74×10^{-3} at $R =$
11 9.61×10^4 . Consequently, the current study is in agreement with the general consensus that λ
12 for a biofouled surface does not follow the traditional C-W relationship (Barton, 2006).
13
14
15
16

17
18 [Insert Fig. 7]
19

20
21 The degree at which λ increases with R is seemingly a function of the biofilm's
22 overall effective roughness (and thus its roughness distribution). In particular, the greater the
23 roughness, the greater the increase in λ . Lambert et al. (2009) reported a similar phenomenon
24 for biofouling, albeit for smaller diameter pipes (i.e. $D = 25$ -50 mm).
25
26

27 Once the local maximum was reached, λ begins to decrease with increasing R . In the
28 case of the $R = 5.98 \times 10^4$ assay, this decrease was significant; whereas the equivalent decrease
29 in the $R = 1.00 \times 10^5$ assay was far more gradual. Similar trends have been reported within the
30 literature (Barton et al., 2008; Lambert et al., 2009; Perkins et al., 2014). For instance, Perkin
31 et al. (2014) found that the λ of a biofilm incubated in a hydropower pipeline increased
32 gradually with increasing R between $9.32 \times 10^4 < R < 1.57 \times 10^5$, to a maximum of 0.033,
33 before decreasing significantly with increasing R between $1.57 \times 10^4 < R < 2.66 \times 10^5$. The
34 biofilm assessed by Perkin et al. (2014) was conditioned at $\bar{U} = 1.30 \text{ ms}^{-1}$. The evident
35 reduction in λ with R after the local maximum was reached could be explained by a reduction
36 in biofilm thickness caused by the biofilm compressing itself under loading (Percival, Knapp,
37 Wales, & Edyean, 1999), or by it being sheared from the surface (Andrewartha, 2010;
38 Barton, 2006). The usual reduction in λ with R could also explain the evident trend (Perkin et
39 al., 2014).
40
41
42
43
44
45
46

47 The concentration of TOC in the bulk water was measured at each R increment to
48 indirectly determine whether the increase in flow shear could actively remove the biofilm
49 from the surface. Bulk water samples were taken directly from the storage tank and stored at
50 20°C before being analysed. Due to the relatively short time it took to complete each of the
51 mature testing phases (i.e. < 15 h), any changes in water chemistry during this phase would
52 have likely been caused by biofilm detachment. The concentrations of TOC recorded in the
53 bulk water for the $R = 5.98 \times 10^4$ and $R = 1.00 \times 10^5$ assays is presented in Fig. 8. It is evident
54 from Fig. 8 that the concentration of TOC increased significantly in the $R = 5.98 \times 10^4$ assay as
55
56
57
58
59
60

1
2
3 flow shear increased. In particular, a significant increase in TOC was evident when R
4 exceeded 6.54×10^4 . The equivalent increase was less extreme in the $R = 1.00 \times 10^5$ assay,
5 although an increase was evident when R exceeded 9.60×10^4 . The observed increases in
6 organic content in each assays' bulk water suggests that biofilm detachment was likely to
7 have occurred. However, based on the magnitude of the respective increases, the degree of
8 detachment will have varied between the assays. For instance, the concentration of TOC in
9 the bulk water of the $R = 5.98 \times 10^4$ assay following the increase in flow shear was 62.5 mg l^{-1} ,
10 whereas the equivalent concentration in the bulk water of the $R = 1.00 \times 10^5$ assay was 10.9
11 mg l^{-1} . Therefore, it could be suggested that greater biofilm detachment was likely to have
12 occurred in the $R = 5.98 \times 10^4$ assay than in the $R = 1.00 \times 10^5$ assay. The presumed detachment
13 point for the $R = 1.00 \times 10^5$ assay's biofilm, as suggested by the increase in bulk water organic
14 content, is the same point at which a reduction in λ was first recorded (see Fig. 7).
15
16
17
18
19
20
21
22

23 *[Insert Fig. 8]*
24
25

26 The gradual reduction in λ combined with the relatively low increase in TOC with R ,
27 which was observed in the $R = 1.00 \times 10^5$ assay, could potentially suggest that the respective
28 biofilm was merely thinned and/or compressed by the increase in flow shear. Alternatively,
29 the considerable changes in λ and TOC observed in $R = 5.98 \times 10^4$ assay, would suggest that
30 large scale detachment occurred in the respective assay. However, as λ did not approach the
31 non-fouled curve post shear, it was unlikely that the biofilm was completely removed. The
32 point at which λ began to decrease with R in the $R = 5.98 \times 10^4$ assay did not coincide with the
33 detachment point implied by the changes in bulk water chemistry (i.e. $R > 6.54 \times 10^4$). In fact,
34 λ continued to increase beyond this presumed detachment point; and this suggests that biofilm
35 detachment did not occur. However, it is possible that the initial detachment which gave rise
36 to the increases in bulk water organic content had a negligible effect on the biofilm's
37 frictional capacity. Conversely, it is equally possible that the initial biofilm detachment could
38 have given rise to a more heterogeneous roughness distribution, which could have directly
39 contributed to, or be the reason for the observed λ relationship.
40
41
42
43
44
45
46
47

48 3.4 Determining κ for biofouled surfaces

49 The von Kármán constant's dependence on R was assessed using the PG and mean-velocity
50 data recorded during the mature testing phase. In particular, a linear regression line of best fit
51 was fitted to the log-law region of U^+ against $\ln((y+\epsilon)/k_s)$ plot. The inverse of the slope of this
52 regression line was equal to κ (i.e. $\kappa = 1/[d(U^+)/d(\ln((y+\epsilon) u_* / \nu))]$). The location of the log-law
53 region within the boundary layer was determined experimentally using the method outlined
54
55
56
57
58
59
60

1
2
3 by Saleh (2005), and it was found to be unaffected by the presence of a biofilm. The location
4 of the log-law region was taken as $50 < yu_* / \nu < 0.18r^+$ ($= r\nu / u_*$) which is also where standard
5 convention states that it should be (George, 2007).
6

7
8 Wall similarity techniques, such as the PL method are typically used to determine
9 local frictional conditions at a particular streamwise location from mean-velocity data.
10 However, such techniques are inherently dependent on a universal log-law in which κ is a
11 known constant and typically equal to 0.42. As κ is the unknown in this instance, wall
12 similarity techniques cannot be applied. Therefore, with no other means of determining the
13 local frictional data, the global data determined from the system's PG was used. In particular,
14 the frictional data determined between P_3 and P_5 was applied in this case. It should be noted
15 that although the global values of u_* were unaffected by κ , the global values of k_s required re-
16 calculation using Eq. (5). This was an iterative process that typically required 3-4 iterations
17 for a suitable convergence to be obtained.
18

19
20 Despite the fact that the applied global data represents the frictional conditions for the
21 section at which the mean-velocity data was recorded, it may not be a true reflection of the
22 local frictional conditions at P_5 (i.e. where the mean-velocity data was recorded). This is
23 because a biofilm's roughness distribution is generally heterogenetic, as highlighted by the
24 biofilm incubated in the $R = 5.98 \times 10^4$ assay. Furthermore, although the biofilm incubated in
25 the $R = 1.00 \times 10^5$ assay displayed a seemingly uniform roughness distribution, it is still highly
26 unlikely that it was truly homogeneous over the whole system. Any error in the frictional data
27 used to determine κ would naturally result in errors in established values κ (Wei et al., 2005).
28 Consequently, the results presented herein should be viewed accordingly and with caution.
29

30
31 The relationship between κ and R is presented in Fig. 9 which illustrates the
32 combined data measured in the two fouled pipes. As it was not possible to distinguish
33 between the two fouled pipe's datasets, the two datasets were combined. It is evident from
34 Fig. 9 that κ has a dependency on R , and in particular, a trend of increasing κ with increasing
35 R can be observed. The elastic nature of a biofilm may have contributed to these trends. The
36 lowest value of κ was measured for $R = 2.50 \times 10^5$ and it was equal to 0.32. The reduction in κ
37 from the conventional value lessened as R increased. This may have been as a result of the
38 assumed biofilm detachment and the smoothening of the pipe's surface under loading. This is
39 supported by the fact that the value of κ approaches the canonical value as R increases.
40

41
42
43
44
45
46
47
48
49
50
51
52
53
54
55
56
57
58
59
60
[Insert Fig. 9]

The relationship of κ with R was found to be a linear function ($R^2 > 0.95$), as given
by:

$$\kappa = 9.443 \times 10^{-7}R + 0.302 \quad (7)$$

The trend observed within the current study for κ is consistent with the findings of Perkins et al. (2014) and Lambert et al. (2009). However, the values of κ found within the current study were generally higher than the equivalent values reported by Perkins et al. (2014), who assessed the impact of biofouling on κ in a pipe with similar diameter to that used within the current study (i.e. $D = 101.6\text{mm}$). Nonetheless, the biofilms observed by Perkins et al. (2014) had a significant filamentous component. Visually, the filaments pictured by Perkins et al. (2014) were considerably more abundant than those observed within the current study. Filamentous type development is known to induce a considerable amount of drag on a system, and it can alter the mean flow structure in the outer region of the boundary layer in some extreme cases (Andrewartha, 2010; Barton et al., 2006). However, as a result of the inherently dark conditions in a DN, it is unlikely that the filaments observed by Perkins et al. (2014) would have been as long as those reported in the extreme cases, which typically relate to biofilms incubated in open channels. Nevertheless, the interactions between the filaments and the fluid may have contributed to the lower values of κ observed by Perkins et al. (2014). Consequently, the degree and type of biofouling may have had a greater influence on κ than was first thought, based on the observations reported within this study.

The observed non-universality of κ means that as expected, the values of k_s derived using Eq. (3), and presented in Table 3 are unrepresentative of the actual conditions. The equilibrium state values of k_s as derived from Eq. (5) (where κ is defined by Eq. 7) for the $R = 5.98 \times 10^4$ and $R = 1.00 \times 10^5$ assays were 0.11mm and 0.08mm , respectively. Therefore, the traditionally derived k_s values (see Table 3) are significantly higher than those derived using the modified C-W equation. Nevertheless, although the magnitude of the k_s values may have changed, the influence of conditioning shear on biofilm induced k_s remained the same. Figure 10 presents the experimentally determined mature phase values of λ recorded in the $R = 5.98 \times 10^4$ and $R = 1.00 \times 10^5$ assays, along with theoretically determined values derived from Eq. (5) and (7). It is evident from Fig. 10 that prior to the local maximums being reached, the modified C-W curves established using Eq. (5) and (7) were in good agreement with the experimentally determined values of λ . In particular, it was found that the maximum discrepancy between the measured and predicted values was $\pm 7.21\%$. The average discrepancy between the respective values of λ was $\pm 2.82\%$. These discrepancies are within the experimental uncertainty in λ presented in Table 2.

[Insert Fig. 10]

1
2
3 The suggestion that wall similarity applies to biofouled pipes (i.e. as indicated by Fig.
4 5) can also be questioned by the observed non-universality of κ . This is because the velocity
5 defect plots presented in Fig. 5 were scaled by values of u_* derived from the PL method.
6 Velocity defect plots, which have been scaled by values of u_* determined directly from the
7 system's PG are presented in Fig. 11 for the $R = 5.98 \times 10^4$ and $R = 1.00 \times 10^5$ assay. The
8 observed collapses of the non-fouled and fouled profiles suggest that wall similarity is valid
9 for biofouled surfaces, irrespective of the non-universality of the log-law constants.
10
11
12
13

14
15 *[Insert Fig. 11]*
16
17
18
19

20 **4 Conclusions and recommendations**

21 *4.1 Conclusions*

22
23 Biofouling in drainage networks is realistically unavoidable. Therefore, the frictional
24 properties of a biofilm, which are characterised by their highly dynamic and case-specific
25 nature, should represent the “true” underlying surface roughness of all pipelines in service.
26 However, such an understanding is currently not recognised within conventional design
27 practices, and this is detrimental to efficient and sustainable operation given that:
28
29
30
31

- 32 • a biofilm has an inherent ability to induce an effective roughness which is well in
33 excess of what its physical structure would traditionally suggest; and
- 34 • traditional frictional relationships fail to adequately account for the true nature of a
35 biofouled surface in their current manifestation.
36
37
38
39

40 The current study has comprehensively evaluated the impact of biofouling on
41 frictional resistance of a high density polyethylene drainage pipe. The finding of the study
42 with regards to the influence of flow hydrodynamics on biofilm frictional development over
43 time, have gone beyond that previously documented within the literature.
44
45

46 An initial increase in roughness caused by biofilm development was observed after
47 just 25 h of incubation, and it continued to increase until a statistically steady state was
48 achieved. The time at which the biofilms reached a state of equilibrium was found to be
49 independent of the conditioning shear and equal to 180 h. The magnitude of a biofilm's
50 frictional resistance was evidently a function of the shear conditions under which the biofilm
51 was incubated. Most notably, it was found that the lower the conditioning shear, the higher
52 the frictional resistance imparted by the biofilm. This is attributed to the thickness and
53 roughness distribution induced by such conditions, and it serves to highlight the problem of
54
55
56
57
58
59
60

1
2
3 characterising a biofilm's effective roughness using a single roughness scale. A biofilm's
4 impact on frictional resistance is further compounded by its influence over the von Kármán
5 constant. In particular, the current study has provided conclusive evidence that the von
6 Kármán constant for biofouled surfaces is non-universal, dependent on Reynolds number, and
7 lower than the conventionally accepted value. As a consequence of the non-universality of the
8 von Kármán constant, the traditional Colebrook-White equation is not applicable to biofouled
9 pipes. The Darcy-Weisbach friction factor for a biofouled surface was shown to increase with
10 increasing Reynolds number, until a critical threshold was reached. Thereafter, the Darcy-
11 Weisbach friction factor decreased with increasing Reynolds number. This decrease was
12 partly attributed to the biofilm becoming detached under loading. Changes in bulk water
13 chemistry, and in particular organic content supported this assumption.

14
15 A modified Colebrook-White equation (i.e. Eq. (3)) can be applied to drainage
16 networks, provided the von Kármán constant is defined by Eq. (7). Furthermore, it was found
17 that, although wall similarity is valid and applicable to biofouled surfaces, it is reliant on
18 either the von Kármán constant or shear velocity being known, without which the results are
19 likely to be unrepresentative of the actual conditions.

20 21 22 23 24 25 26 27 28 29 *4.2 Recommendations for further research*

30
31 The incubation conditions used within the current study were purposely designed to
32 be representative of those found within natural sewer systems, albeit for those operating at
33 full bore. The resultant biofilms incubated and evaluated within this study can therefore be
34 considered equivalent to those found in real systems. However, wastewater systems with the
35 exception of rising mains are rarely operated at full bore, and drainage networks as a whole
36 are generally unsteady in nature. Consequently, although the study has provided much needed
37 data on biofouling in DNS, further research is still required in order for biofouling to be truly
38 incorporated in pipeline design practices. Such research should ideally expand on the
39 fundamental ideas and concepts outlined within this study. In particular, it is recommended
40 that biofilm development over time is evaluated for a greater range of conditions including a
41 broader range of flow regimes, nutrient levels, operating depths and temperatures. Similarly,
42 given the highly variable nature of real systems, it would be beneficial to incorporate and
43 evaluate typical daily and seasonal variations in operational and environmental conditions
44 within future studies. This study has however provided the platform and methodology needed
45 for such future investigations to be achieved

54 55 **Acknowledgements**

56
57 The authors would like to thank Dr Gordon Webster (Cardiff University) for his support and
58
59
60

guidance on the molecular analysis aspect of this study. The industrial insight and expertise provided by Dr Vasilios Samaras (Asset International Limited) should also be acknowledged. Furthermore, Dr William Rauen (Universidade Positivo, Brazil) and Professor Binliang Lin (Tsinghua University, China) must be accredited for the initial research concept. The authors would also like to thank the technical staff at the School of Engineering, Cardiff University, and in particular, Mr Len Czekaj and Mr Paul Leach for their support with the experimental work. Finally, the authors would like to thank Mr Mark Taylor (Mott MacDonald) for taking the time to review the manuscript.

Funding

This work was supported by the UK Engineering and Physical Sciences Research Council (EPSRC) and Asset International Limited.

Notation

B = Nikuradse's roughness function

c_f = local skin friction coefficient

D = pipe diameter (mm)

d_c = diameter of the pressure transducer connection tube (mm)

d_h = wall tapping hole diameter (mm)

d_p = Pitot Probe diameter (mm)

g = gravity acceleration constant (ms^{-2})

h = hours

H_f = hydraulic head (mm)

k_s = Nikuradse-type equivalent sandgrain roughness (mm)

L = streamwise Length (m)

ΔP = pressure drop (Nm^{-2})

Q = volumetric flow rate (m^3s^{-1})

r = pipe radius (mm)

R^2 = coefficient of determination

R = Reynolds number

S_f = friction slope

T = temperature ($^{\circ}\text{C}$)

t = time (h)

\bar{U} = area-averaged axial velocity (ms^{-1})

u = local mean streamwise velocity (ms^{-1})

U^+ = normalised velocity

1
2
3 $u_* =$ wall shear velocity (ms^{-1})
4 $\Delta U^+ =$ Hama's (1954) roughness function
5
6 $x =$ characteristic length scale
7
8 $y =$ distance from the wall (mm)
9
10 $\Delta =$ change in a variable
11 $\varepsilon =$ wall origin error (mm)
12 $\kappa =$ von Kármán constant
13 $\lambda =$ Darcy-Weisbach friction factor
14
15 $\mu =$ dynamic viscosity (Nm^{-2}s)
16
17 $\rho =$ density (kgm^{-2})
18
19 $\tau_w =$ wall shear stress (Nm^{-2})
20
21 $\nu =$ kinematic viscosity (m^2s^{-1})
22
23 $^+ =$ normalised by u_* or u_*/ν

24 References

- 25
26 Andrewartha, J. M. (2010). *The effect of freshwater biofilms on turbulent boundary layers*
27 *and the implications for hydropower canals* (PhD thesis). University of Tasmania
28 (UTAS), Australia.
29
30
31 Barton, A. F. (2006). Friction, roughness and boundary layer characteristics of freshwater
32 biofilms in hydraulic conduits (PhD thesis). University of Tasmania (UTAS), Australia.
33
34 Barton, A. F., Wallis, M. R., Sargison, J. E., Buia, A. & Walker, G. J. (2008). Hydraulic
35 roughness of biofouled pipes, biofilm character, and measured improvements from
36 cleaning. *Journal of Hydraulic Engineering*, 134 (6).
37
38 Celmer, D., Oleszkiewicz, J. & Cicek, N. (2008). Impact of shear force on the biofilm
39 structure and performance of a membrane biofilm reactor for tertiary hydrogen-driven
40 denitrification of municipal wastewater. *Water Research*, 42(12), 3057-3065.
41
42 Cipolla, S. S. & Maglionico, M. (2014). Heat recovery from urban wastewater: Analysis of
43 the variability of flow rate and temperature. *Energy and Buildings*, 69, 122-130.
44
45 Cowle, M.W, Babatunde, A.O, Rauen, W.B, Bockelmann-Evans, B.N & Barton, A.F (2014)
46 Biofilm development in water distribution and drainage systems: dynamics and
47 implications for hydraulic efficiency. *Environmental Technology Reviews*, 4(1), 31-47.
48
49 George, W. K. (2007). Is there a universal log law for turbulent wall-bounded flows?
50 *Philosophical Transactions of the Royal Society A: Mathematical, Physical and*
51 *Engineering Sciences*, 365(1852), 789-806.
52
53
54
55
56
57
58
59
60

- 1
2
3 Lambert, M. F., Edwards, R. W. J., Howie, S. J., De Gilio, B. B. & Quinn, S. P. (2009). The
4 impact of biofilm development on pipe roughness and velocity profile. *Proceedings of*
5 *the World Environmental and Water Resources Congress 2009*, Kansas City, Missouri.
6
7 Lauchlan, C., Forty, J. & May, R. (2005). Flow resistance of wastewater pumping mains.
8 *Water management*, 158(2), 81-88.
9
10 Ligrani, P. M. & Moffat, R. J. (1986). Structure of transitionally rough and fully rough
11 turbulent boundary layers. *Journal of Fluid Mechanics*, 162, 69-98.
12
13 McKeon, B. J. & Smits, A. J. (2002). Static pressure correction in high Reynolds number
14 fully developed turbulent pipe flow. *Measurement Science and Technology*, 13(10),
15 1608-1614.
16
17 McKeon, B. J., Li, J., Jiang, W., Morrison, J. F. & Smits, A. J. (2003). Pitot probe corrections
18 in fully developed turbulent pipe flow. *Measurement Science and Technology*, 14(8),
19 1449-1458.
20
21 Nikuradse, J. (1933). Laws of flow in rough pipes. *Mechanical Engineering Papers*, 1292(1),
22 1-62.
23
24 OECD (1984). Activated sludge, respiration inhibition test. Organisation for Economic
25 Cooperation and Development (OCED) Guidelines. *In Testing Chemicals* 1-10.
26
27 Percival, S. L., Knapp, J. S., Wales, D. S. & Edyvean, R. G. J. (1999). The effect of turbulent
28 flow and surface roughness on biofilm formation in drinking water. *Journal of*
29 *industrial microbiology & biotechnology*, 22(3), 152-159.
30
31 Perkins, S., Henderson, A., Walker, J., Sargison, J. & Li, X. (2014). The influence of bacteria-
32 based biofouling on the wall friction and velocity distribution of hydropower pipes.
33 *Australian Journal of Mechanical Engineering*, 12(1), 77-88.
34
35 Perry, A. & Joubert, P. (1963). Rough-wall boundary layers in adverse pressure gradients.
36 *Journal of Fluid Mechanics*, 17(2), 193-211.
37
38 Perry, A. & Li, J. D. (1990). Experimental support for the attached-eddy hypothesis in zero-
39 pressure-gradient turbulent boundary layers. *Journal of Fluid Mechanics*, 218, 405-438.
40
41 Saleh, O. A. B. (2005). Fully developed turbulent smooth and rough channel and pipe flows
42 (PhD thesis). Lehrstuhl für Strömungsmechanik, Universität Erlangen-Nürnberg
43
44 Santo Domingo, J. W., Revetta, R. P., Iker, B., Gomez-Alvarez, V., Garcia, J., Sullivan, J. &
45 Weast, J. (2011). Molecular survey of concrete sewer biofilm microbial communities.
46 *Biofouling*, 27(9), 993-1001.
47
48 Stoodley, P., Cargo, R., Rupp, C. J., Wilson, S. & Klapper, I. (2002). Biofilm material
49 properties as related to shear-induced deformation and detachment phenomena. *Journal*
50 *of Industrial Microbiology and Biotechnology*, 29(6), 361-367.
51
52
53
54
55
56
57
58
59
60

- 1
2
3 Stoodley, P., Dodds, I., Boyle, J. D. & Lappin-Scott, H. M. (1998a). Influence of
4 hydrodynamics and nutrients on biofilm structure. *Journal of applied microbiology*,
5 85(S1), 19S-28S.
6
7 Stoodley, P., Lewandowski, Z., Boyle, J. D. & Lappin-Scott, H. M. (1998b). Oscillation
8 characteristics of biofilm streamers in turbulent flowing water as related to drag and
9 pressure drop. *Biotechnology and Bioengineering*, 57(5), 536-544.
10
11 Walker, J., Sargison, J. & Henderson, A. (2013). Turbulent boundary-layer structure of flows
12 over freshwater biofilms. *Experiments in fluids*, 54(12), 1-17.
13
14 Walker, J. (2014). The Application of Wall Similarity Techniques to Determine Wall Shear
15 Velocity in Smooth and Rough Wall Turbulent Boundary Layers. *Journal of Fluids*
16 *engineering*, 136(5), 383-413.
17
18 Wei, T., Schmidt, R. & McMurtry, P. (2005). Comment on the Clauser chart method for
19 determining the friction velocity. *Experiments in fluids*, 38(5), 695-699.
20
21 Zagarola, M. V. (1996). Mean-flow scaling of turbulent pipe flow (PhD thesis). Princeton
22 University, Princeton, NJ.
23
24 Zagarola, M. V. & Smits, A. J. (1998). Mean-flow scaling of turbulent pipe flow. *Journal of*
25 *Fluid Mechanics*, 373, 33-79.
26
27
28
29
30
31
32
33
34
35
36
37
38
39
40
41
42
43
44
45
46
47
48
49
50
51
52
53
54
55
56
57
58
59
60

Table Captions

Table 1 Physico-chemical properties of the synthetic wastewater used within the $R = 5.98 \times 10^4$, $R = 7.82 \times 10^4$ and $R = 1.00 \times 10^5$ assays.

Table 2 Uncertainty estimates derived from the evaluation of the non-fouled pipe over the range of $3.15 \times 10^4 < R < 1.23 \times 10^5$.

Table 3 Average frictional data determined from the system's PG at $t > 180$ h (i.e. during the equilibrium stage).

Figure Captions

Figure 1 Perspective 3-D view of the pilot scale pipeline (the flow direction is clockwise).

Figure 2 Schematic of the 8.5 m test section of the pilot scale pipeline, highlighting the pressure tapping locations and general arrangement.

Figure 3 Influence of biofilm development over time on λ within the $R = 5.98 \times 10^4$, $R = 7.82 \times 10^4$ and $R = 1.00 \times 10^5$ assays.

Figure 4 Normalised mean-velocity profiles for the $R = 5.98 \times 10^4$ and $R = 1.00 \times 10^5$ assays at (a) $0 < t$ (h) < 25 , (b) $25 < t$ (h) < 180 and (c) t (h) > 180 .

Figure 5 Velocity defect plots for the $R = 5.98 \times 10^4$ and $R = 1.00 \times 10^5$ assays at $t > 180$ h (i.e. the during equilibrium stage).

Figure 6 Standard deviation in space-averaged λ along the length of the Test Section for the $R = 5.98 \times 10^4$ and $Re_D = 1.00 \times 10^5$ assays.

Figure 7 The influence of R on λ , for the mature biofilms incubated within $R = 5.98 \times 10^4$ and $R = 1.00 \times 10^5$ assays.

Figure 8 Concentration of TOC within the bulk water against R , for $R = 5.98 \times 10^4$ and $R = 1.00 \times 10^5$ assays.

Figure 9 Relationship of κ with R for the biofouled pipes.

Figure 10 Experimentally and theoretically determined values λ against R for the biofilm incubated within the $R = 5.98 \times 10^4$ and $R = 1.00 \times 10^5$ assay. The theoretically determined values were derived from the Eq. (3) and Eq. (7).

1
2
3
4
5
6
7
8
9
10
11
12
13
14
15
16
17
18
19
20
21
22
23
24
25
26
27
28
29
30
31
32
33
34
35
36
37
38
39
40
41
42
43
44
45
46
47
48
49
50
51
52
53
54
55
56
57
58
59
60

Figure 11 Velocity defect plots scaled using the global values of u_* for the $R = 5.98 \times 10^4$ and $R = 1.00 \times 10^5$ assays, at $t > 180$ h (i.e. during the equilibrium stage).